ACS APPLIED MATERIALS & INTERFACES

Research Article

www.acsami.org

Patterning Cellular Alignment through Stretching Hydrogels with Programmable Strain Gradients

Lin Wang,[†,‡,⊥] Yuhui Li,[†,‡,⊥] Bin Chen,[∥] Shaobao Liu,[‡] Moxiao Li,[‡] Lu Zheng,[†,‡] Pengfei Wang,[‡,§] Tian Jian Lu,[‡] and Feng Xu*[,†,‡]

[†]MOE Key Laboratory of Biomedical Information Engineering, School of Life Science and Technology and [‡]Bioinspired Engineering and Biomechanics Center (BEBC), Xi'an Jiaotong University, Xi'an 710049, People's Republic of China

[§]Qian Xuesen Laboratory of Space Technology, China Academy of Space Technology, Beijing 100094, People's Republic of China

[∥]Department of Engineering Mechanics, Zhejiang University, Hangzhou 310027, People's Republic of China

Supporting Information

ABSTRACT: The graded mechanical properties (e.g., stiffness and stress/strain) of excellular matrix play an important role in guiding cellular alignment, as vital in tissue *reconstruction with proper functions*. Though various methods have been developed to engineer a graded mechanical environment to study its effect on cellular behaviors, most of them failed to distinguish stiffness effect from stress/strain effect during mechanical loading. Here, we construct a mechanical environment with programmable strain gradients by using a hydrogel of a linear elastic property. When seeding cells on such hydrogels, we demonstrate that the pattern of cellular alignment can be rather precisely tailored by substrate strains. The experiment is in consistency with a theoritical prediction when assuming that focal adhesions (FAs) would drive a cell to reorient to the directions where they are most stable. A fundamental theory has also been developed and is excellent in agreement with the complete temporal alignment of cells. This work not only provides important insights into the cellular response to the local mechanical microenvironment but can also be utilized to engineer patterned cellular alignment that can be critical in tissue remodeling and regenerative medicine applications.

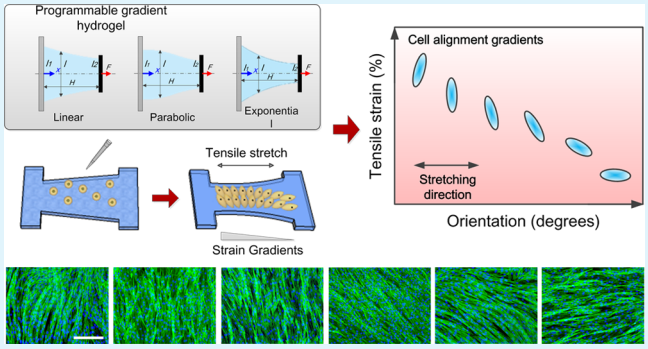

KEYWORDS: *gradient hydrogels, programmable, cellular alignment, stress/strain, stiffness*

1. INTRODUCTION

Cellular alignment, which refers to spatial and oriented organization of cells,[1,2] plays a critical role in pattern formation during embryogenesis,[3] tissue maturation,[4] and regeneration.[5,6]. The formation of cellular alignment in vivo is generally accompanied by differentiation,[7] proliferation,[8] and the changes of physical cues in the surrounding cellular microenvironment.[9,10] It can further lead to the formation of various alignments of subcellular structures, including plasma membrane, cytoskeleton, and cell-adhesion complexes.[11] Additionally, cellular alignment combined with proliferation, migration, and secretion of structural substances determines the hierarchy of cells and tissues, providing the physical and mechanical properties and special biological functions at tissue levels.[12] Aligned organization of cells also results in secretion and deposition of a highly anisotropic extracellular matrix (ECM), which is specific to tissue type and critical in determining tissue function.[13] Therefore, it is essential to pattern cellular alignment in vitro to regenerate structured and functional tissue equivalents.

It is well-known that cellular behaviors in vivo are regulated by mechanical properties of ECM7,[14,15] e.g., stiffness and stress/strain, mostly in the format of spatiotemporal gradients.[16−19] For instance, one common mechanical cue that cells experience in vivo is the stiffness gradients of extracellular matrix (ECM), ranging from ∼0.1 kPa in soft tissues such as brain tissues to ∼20 kPa in hard tissues such as bones.[5] Another example is that shear stress gradients generated by changes in vascular wall sizes can induce circumferential alignment of smooth muscle cells in the form of a fibrous helix within vascular media, collagen fibers stacked between bands of elastin, or discontinuous sheets of endothelial basement membrane.[20−22] In heart muscles, native ventricular myocardium, composed of sheets of aligned cardiac fibers and myocytes, is formed due to local tensile stress gradients, which can have a strong ductility for heart beating.[23] Therefore, it is important to study how cellular behaviors in vitro are influenced by the graded mechanical environment. Indeed, it was already found that graded mechanical environment played

Received: May 22, 2015
Accepted: June 16, 2015
Published: June 16, 2015

DOI: 10.1021/acsami.5b04450
ACS Appl. Mater. Interfaces 2015, 7, 15088−15097

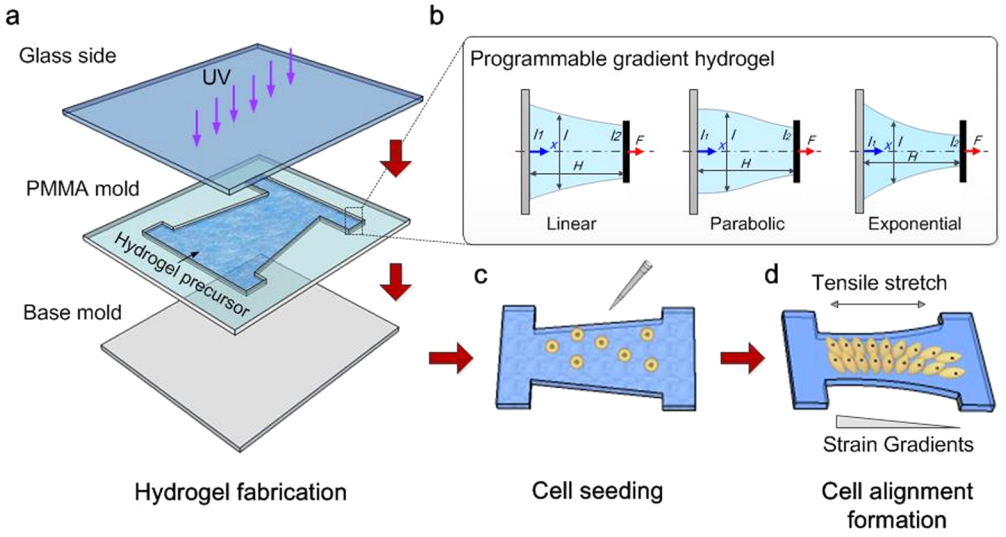

Figure 1. Schematics of fabrication method for hydrogels with stress/strain gradients. (a) Hydrogels with designed trapezoidal shape are fabricated with PMMA mold through an UV cross-linking reaction. (b) Hydrogels with programmable gradients including linear, parabolic, and exponential. (c) Cells are seeded onto gradient hydrogels. (d) Cells respond to hydrogels with and without stress/strain gradients.

an essential role in regulating in vitro cellular alignment in tissue remodeling and regenerative medicine applications.[24,25]

To mimic cellular behavior in native graded mechanical environment, various cell culture models have been established with hydrogels due to their high water content and biocompatibility, as well as tunable chemical and physical properties.[26−28] Quite a few methods have been developed to generate mechanical gradients in hydrogels, such as microfluidic and photolithography methods.[29−31] For microfluidics, concentration gradients of polymer precursors are generated by a diffusion process generated in microfluidic channels and then stabilized by the appropriate cross-linking reaction, resulting in the gradient of hydrogel monomer fraction and thus stiffness. For photolithography, graded photomask (i.e., masks with gradient UV light transmitted patterns) is used to generate gradients in cross-linking density of polymer networks and thus stiffness. Although various hydrogels with stiffness gradients can be fabricated using these methods, it is still challenging to engineer stress/strain gradients in vitro, which exist within physiologic processes, such as gut peristalsis and heart contraction.[32−35] This is mainly because the effects of stiffness and stress/strain are often intertwined, where the stiffness of hydrogels will change during mechanical loading due to the intrinsic nonlinear mechanical property of most hydrogels.[36] It is challenging to distinguish which stimulus, stiffness or stress/strain, predominantly regulates cellular behaviors (e.g., cellular alignment) with existing platforms. Although several approaches can offer a pure unistrain environment that can clarify the contribution of strain easily, they have limited ability to form a cellular environment with gradual strain gradients, which are important in guiding cell fate in vivo.[37−39] Currently, there is a strong demand for a simple and controllable method to engineer hydrogels with stress/strain gradients without involving significant changes of stiffness.

In this study, we develop a simple and feasible strategy to fabricate hydrogels with strain gradients ranging from 0 to 20%, which covers the physiological range of muscle and heart contraction in vivo. The separation of the effect of stiffness from that of strain has been achieved by using the methacrylated gelatin (GelMA) hydrogel which has linear elastic properties in the testing strain range. Hydrogels with programmable strain gradients were formed by UV cross-linking reaction with designed shapes and then applied by static stretch loading. We then found that strain gradients of hydrogels cause a specific alignment of cells seeded on different locations of the hydrogel. By assuming that FAs would drive a cell to reorient to directions where they are most stable, we theoretically predicted the variation of cellular alignment with strain levels on substrate, which was in consistency with experimental observation. This work indicates that cellular alignment can be rather precisely and significantly tailored with the developed method, which holds great potential to impact a wide range of fields, such as mechanosensitivity, tissue engineering and regenerative medicine.

2. EXPERIMENTAL SECTION

2.1. Methacrylated Gelatin Synthesis. In this study, methacrylated gelatin was synthesized as described previously.[40,41] Briefly, type A porcine skin gelatin (Sigma-Aldrich, St. Louis, MO, USA) was mixed at 10% (w/v) into Dulbecco's phosphate buffered saline (DPBS; GIBCO) at 65 °C and stirred until fully dissolved. Methacrylate (MA) was added to the gelatin solution at a rate of 0.5 mL/min under stirred conditions at 50 °C until the target volume was reached, and they were allowed to react for 1−2 h. The fraction of lysine groups reacted was modified by varying the amount of MA present in the initial reaction mixture. Following a 5× dilution with additional warm (40 °C) DPBS to stop the reaction, the mixture was dialyzed against distilled water using 12−14 kDa cutoff dialysis tubing for 1 week at 40 °C to remove salts and methacrylic acid. The solution was lyophilized for 1 week to generate porous foam and stored at −80 °C until further use.

2.2. Gradient Hydrogel Fabrication. Gradient hydrogel was fabricated by using a two-step approach as schematically illustrated in Figure 1. First, a designed trapezoidal shape (6 mm (upper bottom) × 10 mm (lower bottom) × 10 mm (height)) was drawn by AutoCAD 2011a (Autodesk). Then, a poly(methyl methacrylate) (PMMA) mold (Shuguang Plexiglas Co., Ltd., Anqing, China) was etched by a laser machine (Universal VLS2.30, Universal Laser Systems, Scottsdale, AZ, USA). Specifically, PMMA mold was composed of two parts, i.e., the cover mold containing a trapezoidal in the same size of the designed shape with thickness of 1 mm, and the base mold without any framework acting as a support bottom. Two parts were bound using double-sided tape. Then, 750 μL of (15% (w/v)) GelMA precursor solution mixed with 0.05% (w/v) photoinitiaitor (2-hydroxy-2-

DOI: 10.1021/acsami.5b04450
ACS Appl. Mater. Interfaces 2015, 7, 15088−15097

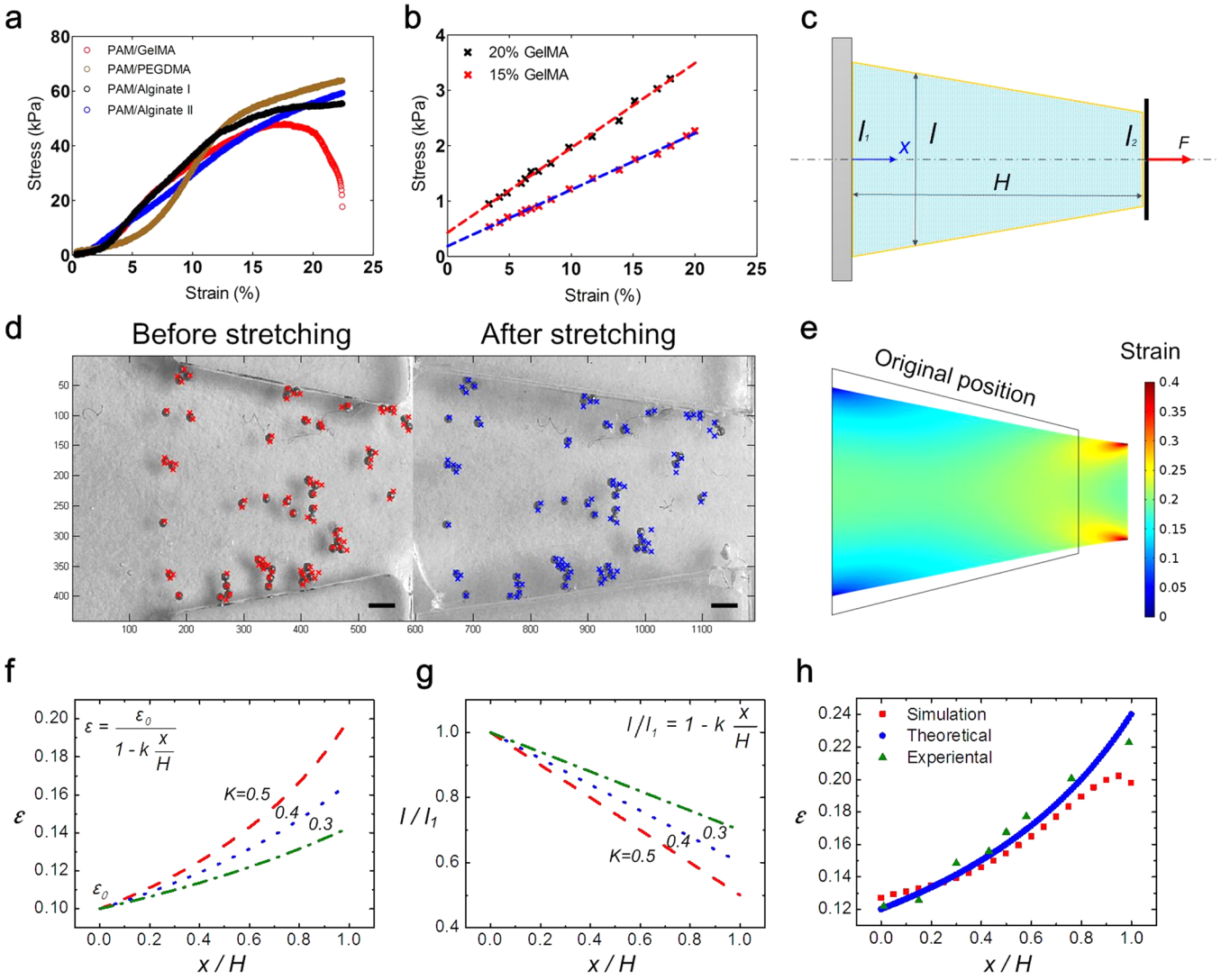

Figure 2. Characterization of strain/stress of different hydrogels. (a) Stress/strain curve of hydrogels including PAM/GelMA, PAM/PEGDMA, and PAM/alginate, in which I and II is in mass ratios 2:1 (w_p/w_g), 1:1 (w_p/w_{peg}), 5:1 (w_p/w_a), and 2:1 (w_p/w_a), respectively. (b) Stress/strain curves of hydrogels with GelMA fraction in 15% and 20% (w/v) (R_1^2 = 0.987, 10% (w/v); R_1^2 = 0.975, 20% (w/v)). (c) Schematics of the curved trapezoid hydrogels. (d) Representative images depict the microbeads used in the texture correlation algorithm before (left) and after (right) stretch to determine strain distribution. (e) FE simulation of strain distribution of hydrogels with inverse gradients. (f) Theoretical distribution of inverse gradients. (g) Shape design of the curved trapezoid for the inverse gradients. (h) Verifications with experimental results and FE simulation for the inverse gradients.

methylpropiophenone H0991; TCI, Shanghai Development Co., Ltd.) was filled into al PMMA mold and coverd with a glass side. The PMMA mold was exposed to UV light (XLE-1000 A/F, Spectroline, Westbury, NY, USA) and polymerized for 25−30 s. Fabricated hydrogels were soaked in PBS solution for 24 h and then used for stretching and cell experiments.

2.3. Mechanical Characterization of Hydrogels. To obtain the stress/strain curves of gradient hydrogels, we used a magnetic-assisted method.[42] Briefly, we encapsulated a magnetically responsive sphere into one side of the hydrogel and another side was fixed on a TMSPMA glass side. Then we applied a magnetic force using a permanent magnet to test stress/strain curves of the GelMA hydrogel. The experimental stress of hydrogel samples was calculated as $\sigma = F/A$, where A represents the initial cross-section area of the hydrogel without mechanical loading and F represents the stretch force testing from Stokes' principle. The engineering strain of the hydrogels was calculated as $\varepsilon = \Delta L/L$, where L is the original length and ΔL is the change of length. The elastic modulus E was determined by taking the slope of the stress versus strain curve in the linear regime between 5% and 20% strain. For other types of hydrogels, including polyacrylamide (PAM)/GelMA (2:1, w_p/w_g), PAM/poly(ethylene glycol) dimethacrylates (PEGDMA) (1:1, w_p/w_{peg}), PAM/alginate I (5:1, w_p/w_a), and PAM/alginate II (2:1, w_p/w_a), the stress/strain curve was tested at a rate of 10% strain/min on an Instron 2360 mechanical tester.

2.4. Analysis of Stress/Strain Distribution on Gradient Hydrogels. To identify spatial stress/strain distribution on gradient hydrogels under stretch loading, we first performed finite element (FE) simulation using COMSOL Multiphysics 4.4a to simulate the strain and stress of stretched gels with different shapes. Due to the much slower diffusion of solvent molecules compared with the experiment process (i.e., the migration of solvent in and out of the hydrogel during the experiment could be ignored), we regarded this material as isotropic and used the soild mechanics interface to simply perform strain and stress analysis. The material properties used in the model are as follows: Young's modulus is 10 kPa (Figure 2a), the Poission ratio is 0.45, and the density is 1000 kg/m^3. The bottom boundary of the hydrogel is fully fixed (no displacements), and the other side is given a prescribed displacement of 2 mm, as was done in the experiment. For experimental images of the strain map of gradient hydrogels, we implemented the scale invariant feature transform

DOI: 10.1021/acsami.5b04450
ACS Appl. Mater. Interfaces 2015, 7, 15088−15097

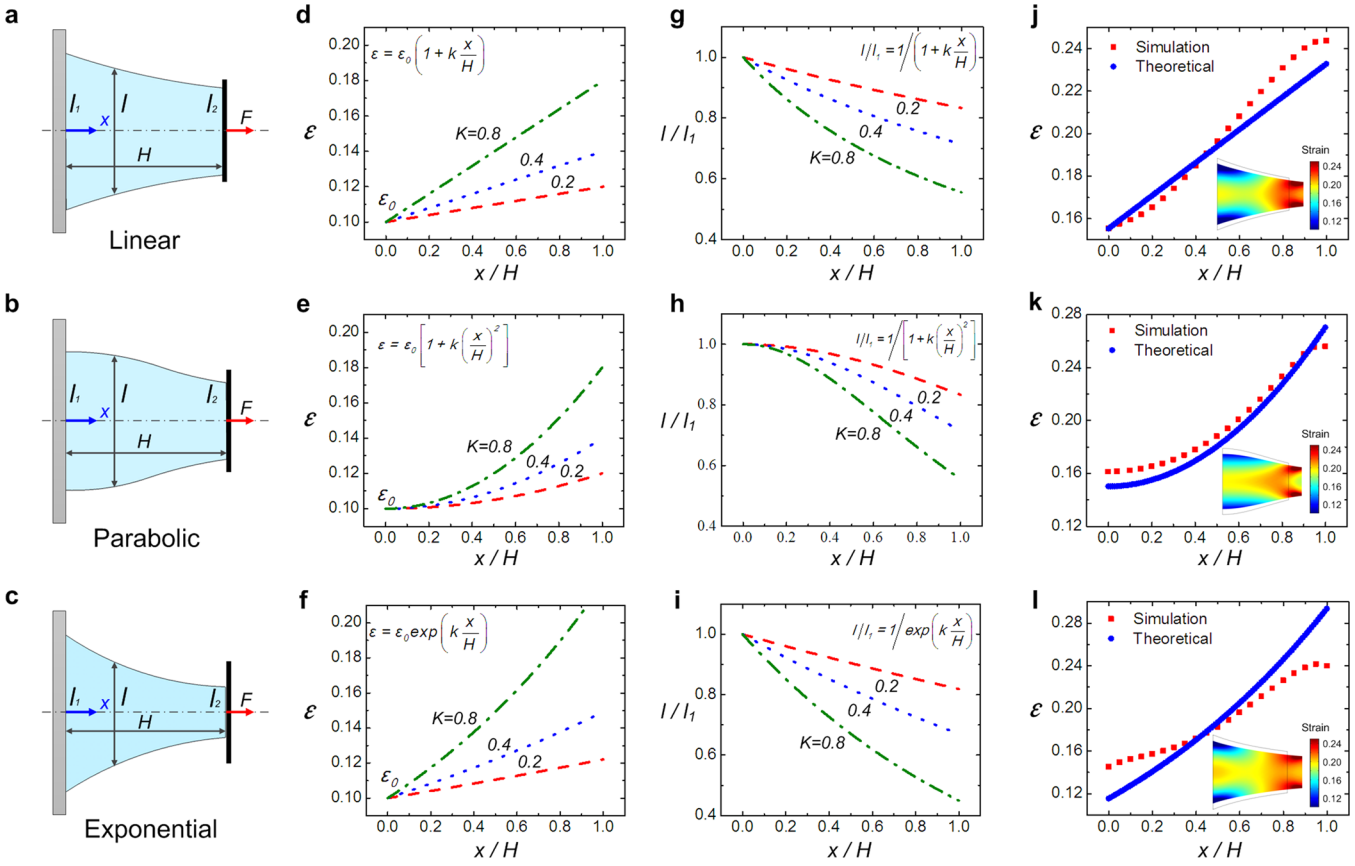

Figure 3. Theoretical and numerical simulation of programmable gradients on hydrogels: (a–c) design of elementary mechanical gradients in a curved trapezoid; (d–f) strain distribution of the linear, parabolic and exponential gradients; (g–i) shape design of the curved trapezoid for the inverse, linear, parabolic, and exponential gradients; (j–l) verifications with theoretical and FE simulation for the inverse, linear, parabolic, and exponential gradients.

(SIFT) method to extract features of iron bead encapsulated in hydrogels, and the positions with salient features were selected.[43] Experimental results of strain distribution in gradient hydrogels were obtained from the microscopy images processing with software Image-Pro Plus (IPP, version 6.0, Media Cybernetics, Silver Spring, MD, USA) and then analyzed using Matlab R2010a.

2.5. Swelling Characterization. Polymerization was performed as described for mechanical testing. Immediately following hydrogel formation, a 16 mm radius disc of each composition was punched from a flat thin sheet and placed in PBS at 37 °C for 24 h. Discs were removed from PBS and blotted with a KimWipe to remove the residual liquid, and the swollen weight was recorded. Samples were then lyophilized and weighed once more to determine the dry weight of polymer. The mass swelling ratio was then calculated as the ratio of swollen hydrogel mass to the mass of dry polymer.

2.6. Cell Preparation and Seeding. The C2C12 cell line from the Cell Bank of the Chinese Academy of Sciences (Shanghai, China) was used in this study. C2C12 cells were cultured in Dulbecco's modified Eagle's medium (DMEM/F-12, GIBCO) supplemented with 10% fetal bovine serum (FBS; GIBCO) and 1% penicillin-streptomycin mixture (GIBCO) at 37 °C in 95% humidity and 5% CO_2. Cells were passaged approximately 2 times per week and media was exchanged every 2 days. Cells were seeded onto gradient hydrogels after hydrogel swelling equilibrium (24 h) (Supporting Information Figure S1a), and cell density was 6×10^5 cells/mL. The culture medium was exchanged after cell adhesion on gradient hydrogels for 2 h and then exchanged every 4 h until four times.

2.7. Cell Fixing and Immunofluorescence Staining. For cellular experiments, F-actin stress fibers and nucleus were stained by FITC conjugated phalloidin (Acti-stain 488 phalloidin, Cytoskeleton, Inc.) and DAPI (Invitrogen). For stress fiber staining, hydrogel samples were first fixed by 4% formaldehyde for 15 min at room temperature and permeabilized in 0.5% Triton X-100 for 5 min. Then, hydrogel samples were washed using PBS for 30 s and covered with 200 μL of 100 nM FITC phalloidin and incubated at room temperature in the dark for 30–40 min. For nucleus staining, 200 μL of 100 nM DAPI was added on hydrogel samples at room temperature for 30 s. The stained hydrogel samples were located on a drop of antifade mounting medium (Invitrogen) on a glass side, which was stored in the dark at 4 °C. All of the fluorescence images were analyzed using Image-Pro Plus.

2.8. Cellular Alignment Analysis. Here, we used an automated method, binarization-based extraction of alignment score, to determine the cell orientation distribution in a wide variety of microscope images, following our previously developed method.[44] This method is composed of a sequential application of locally adaptive thresholding approaches, median and band-pass filters, and image processing techniques. Briefly, quantification of alignment and extraction of overall orientation are implemented in MATLAB 2010a, as follows

$$A(\theta) = \frac{\sum_n T_n \cos(2(\phi - \theta))}{\sum_n T_n} \quad (1)$$

The overall direction of alignment score θ^* was defined as the value of θ that maximized $A(\theta)$. For each angle θ, the degree $A(\theta)$ to which the cells were aligned in the θ direction was calculated by taking the average, weighted by cell size, of the cosine of twice each cell's angle relative to θ.

2.9. Statistical Analysis. All error bars represent standard deviation, with $n = 5$ for both mechanical and structural characterization and $n = 9$ for cell seeding experiments. Student's t-test and paired t-test were used to analyze the statistically significant differences

DOI: 10.1021/acsami.5b04450
ACS Appl. Mater. Interfaces 2015, 7, 15088–15097

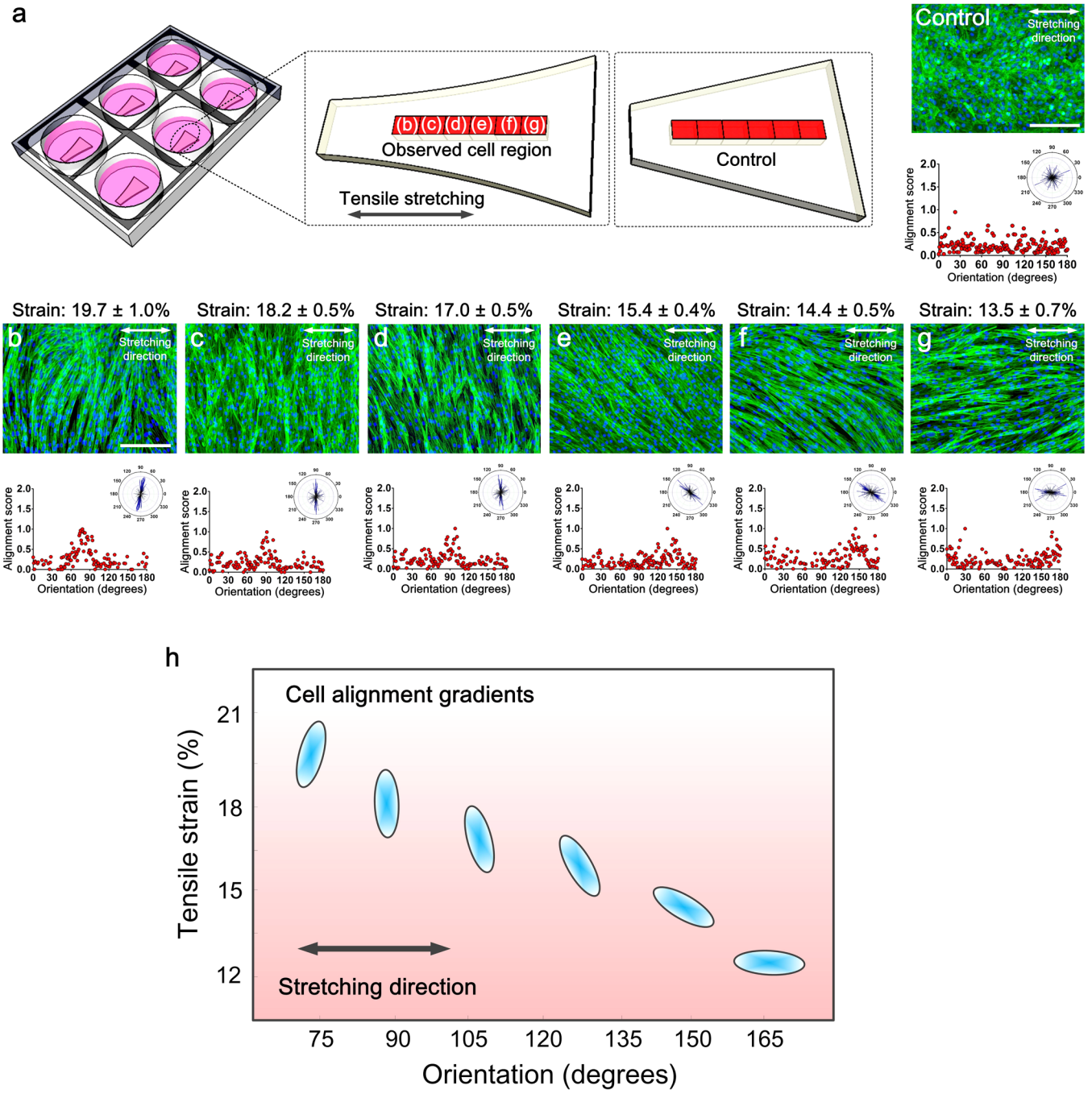

Figure 4. Analysis of cellular alignment generated on gradient hydrogels: (a) schematics of different regions for cellular alignment formation on gradient hydrogels; (b−g) florescent images and quantification of cell orientation on gradient hydrogels with and without (control) stretch loading after 3 days culture (cellular F-actin fibers were stained by phalloidin (green) and nuclei by DAPI (blue); scar bar, 100 μm); (h) profile of cellular alignment under different strains on gradient hydrogels (cellular alignment gradients can be generated on gradient hydrogels with strains ranging from 13% to 20%).

of Young's modulus and cell viability, respectively. Statistical significance threshold was set at 0.05 (i.e., $p < 0.05$) for all tests.

3. RESULTS AND DISCUSSION

Hydrogels with strain gradients were first fabricated using a designed PMMA mold with trapezoid shapes and a simple photolithography method (Figure 1a). As we all know, the stiffness and stress/strain of hydrogels both change when the hydrogels are stretched, especially for large deformation (>10%). To isolate the effects of stiffness and stress/strain, here we used hydrogels of linear elastic properties. To characterize the mechanical properties of prepared hydrogels, tensile stretch tests were performed for hydrogels with GelMA fraction in 15% and 20% both with weak swelling properties (Supporting Information Figure S1), respectively. The stress/strain curve of gradient hydrogels shows a much better linear relationship from 0 to 20% strain, compared with other hydrogels including (PAM)/GelMA, PAM/PEGDMA, and PAM/alginate (Figure 2a,b). These results indicate that the elastic modulus (thus stiffness) of graded hydrogels would not

DOI: 10.1021/acsami.5b04450
ACS Appl. Mater. Interfaces 2015, 7, 15088−15097

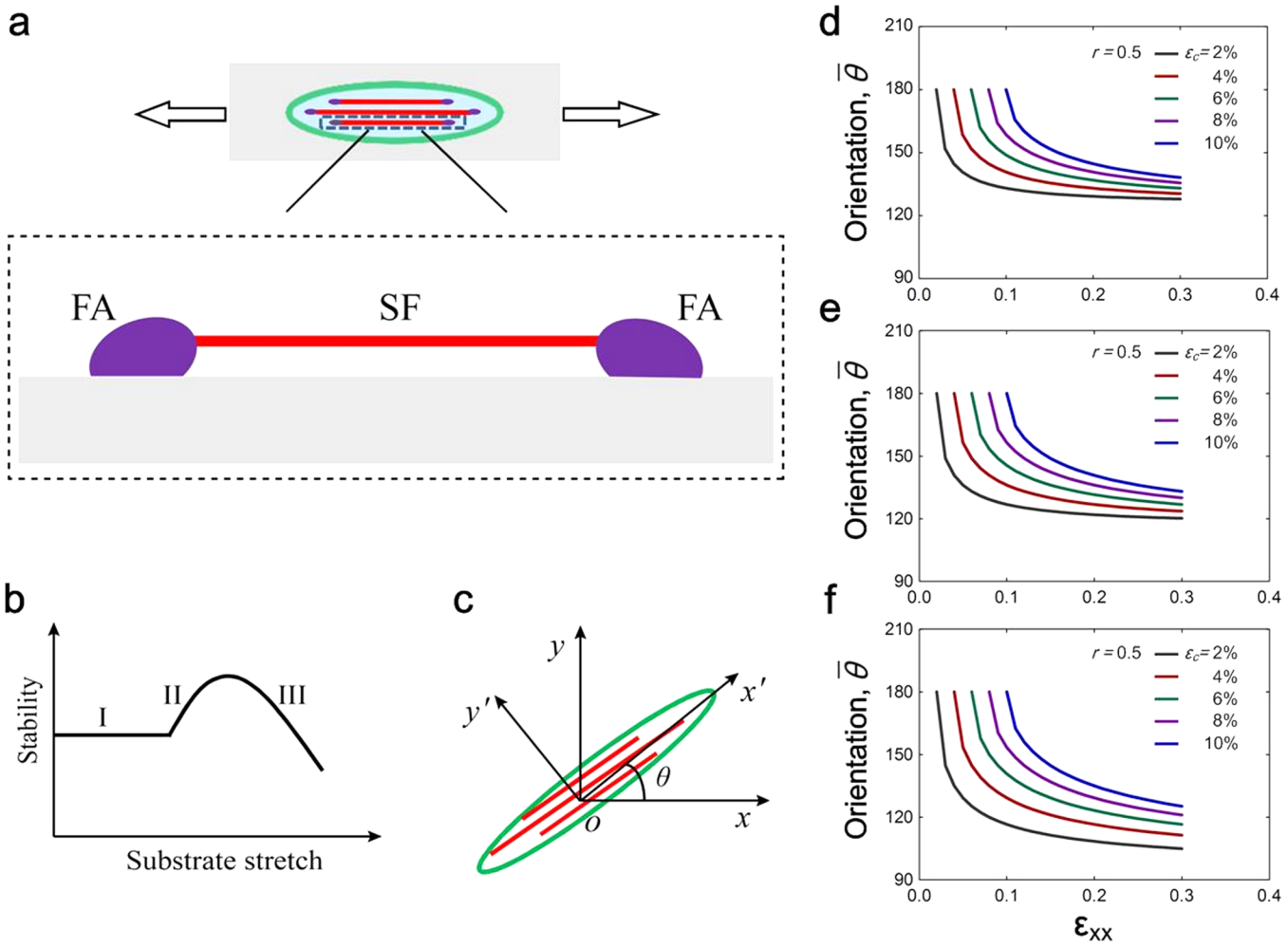

Figure 5. Model of cellular reorientation upon a static stretch. (a) The cellular mechanosensing system on a substrate consists of stress fibers (SFs) adhering on the substrate via FAs. (b) There exist three phases in the response of the stability of FAs to substrate stretch. (c) Schematics of a SF oriented at an angle θ to x axis on substrate. (d–f) These panels illustrate the variation of cellular reorientation with tensile strain on the substrate.

change upon stretch in the range of 0–20% strain, suggesting that we can use this model to distinguish the effect of stiffness from that of stress/strain on cellular behaviors. Young's moduli of 15% and 20% GelMA are 10 and 22 kPa, respectively. In subsequent experiments, 10% GelMA was used, as its mechanical properties are similar to some native soft tissues.[45]

Since there is no significant change of elastic modulus (i.e., stiffness) upon stretch in the range of 0–20% strain, we can theoretically program the stress gradients on hydrogel by designing the specific shape of hydrogel following the relationship: $\sigma = F/A$, where σ represents the stress, F represents the applied force on hydrogel, and A is the original cross-area of the hydrogel. To demonstrate this, we designed hydrogels with inverse strain gradient when a unidirectional load is applied (Figure 2c–h). If the hydrogel is thin and slender, we can consider the trapezoid as a one-dimension structure and thus calculate the shape of the hydrogel. For the sake of convenience, we defined two parameters (ε_0, k) to describe the dimensionless strain gradients that we want, where ε_0 represents the smallest strain at the big bottom of the curved trapezoid and k represents the slope of the strain gradients. Through the reverse operation (see the Supporting Information for details of the derivation process), we can obtain the shape function of the curved trapezoid, as shown in Figure 2g. To verify the designed mechanical gradients, we compared the theoretical strain distribution with the experimental measurement Figure 2d (only the inverse one) and FE simulated results Figure 2e, which has shown a good fit. For Experimental Section, we encapsulated a population of iron beads in hydrogels during the photo-cross-linking process, which were used as markers to determine the spatial distribution of deformation (i.e., strain) on hydrogels under stretching. The typical averaged strain (ε) over the central region in the tension direction could reach up to 20%. According to the theory of nics for homogeneous deformation, the elasticity of gradient hydrogel is determined by the displacement as

$$\varepsilon = \frac{1}{2}[(\nabla u)^T + (\nabla u)] \tag{2}$$

where ε represents the uniform strain of hydrogels and u represents the displacement of the nonboundary hydrogel side. To calculate the strain of gradient hydrogels, we captured the microscopy images of hydrogels with encapsulated iron beads under varying strain.

Following the same strategy, we further designed linear (Figure 3a), parabolic (Figure 3b), and exponential (Figure 3c) strain gradients, since these are the elementary mechanical gradients, combinations of which can generate other gradients. The function and the corresponding strain distribution for these three gradients are shown in Figure 3d–f with the same

DOI: 10.1021/acsami.5b04450
ACS Appl. Mater. Interfaces 2015, 7, 15088–15097

ε_0 = 10% and different slope k. The theoretically calculated strain distributions agree very well with FE simulation, as shown in Figure 3j–l. These results indicate that stress/strain gradient can be designed and fabricated in a programmable manner by stretching hydrogels with designed shapes.

To further confirm the effect of strain gradients in hydrogels substrate on cellular behaviors, the orientation of cells was assessed under static stretch (Figure 4a). Here we chose the hydrogel with inverse strain gradients as a model to study cellular alignment behavior, due to the large strain range formation on hydrogels. We also selected the center area as the observed region to avoid the effect of force concentration in the corners. The cytoskeleton of C2C12 cells (F-actin) seeded on gradient hydrogels was stained at 1, 3, and 5 days during culturing, respectively. Then, we quantified the orientation of cellular stress fiber (Figure 4b–g). The formation of cellular alignment on strained hydrogels at day 3 and day 5 was observed, whereas cells randomly oriented after 1 day culture (Supporting Information Figure S2). The results showed that for a large strain region (17.0 ± 0.5% to 19.7 ± 1.0%) on gradient hydrogels, cells aligned almost perpendicularly to the stretching direction (Figure 4b–d), whereas cells randomly oriented in the control group (nonstretch loading). With decreasing strain from 15.4 ± 0.4% to 13.5 ± 0.7%, stress fibers gradually oriented toward the stretching direction (Figure 4e–g), which is also in agreement with the results shown from the 13% and 10% group without strain gradients (Supporting Information Figure S3a–d). Cells cultured on the nongradient group with 20% strain almost aligned perpendicularly to the stretching direction (Supporting Information Figure S3e). We here successfully created a cellular alignment gradient on the GelMA hydrogel surface under static stretching (Figure 4h), in which the stress gradient generated on hydrogels also ranged from 1.9 ± 0.3 to 3.2 ± 0.1 kPa. These results indicate that cellular response to gradient hydrogels under static stretching is different from the principle that cells orient in the direction of minimal substrate deformation, known as strain-avoidance or stretch-avoidance.[46−48] One possible reason may be the stretch magnitude we applied here is larger than the range shown to induce stretch-avoidence in 2D (<10% strain), which indicated that cell cytoskeleton sensitively responds to high strain. Here we found for the first time that cellular alignment could be formed on gradient hydrogels under static stretch loading, which may provide proof that cell responds differently to small and large strain of their mechanical environments and even in static and dynamic stretch loading state.

To understand how the cellular alignment was tailored by a static stretch on hydrogels, we proposed a model based on the notion that a cell's mechanosensing system on a substrate consists of stress fibers (SFs) adhering on the substrate via FAs[49] (Figure 5a). When the adhered substrate is subjected to a mechanical stretch, the coupled FAs or SF can be further loaded. We regard that there exist three phases in the response of the stability of FAs to a tensile strain on a substrate (Figure 5b). Note that the microstructure of a SF bears significant similarities to that of a skeletal muscle fiber, which would shorten or lengthen depending on applied forces.[49,50] For a relatively small tensile strain, which is at phase I, we regard that the extra force built within the SF can be completely relaxed through its lengthening. At this phase, the force within the SF or on its coupled FAs maintains its isotonic value[49] and there is little effect on the stability of FAs. As the tensile strain on substrate increases, it can be envisaged that the SF would approach its lengthening limit, for example, due to the finite size of sarcomere units,[49] beyond which the force within the SF or on its coupled FAs would then increase almost linearly with the tensile strain. This is termed as phase II. Since FAs are force-responsive and grow in the direction of the force, it will become larger and therefore more stable at phase II.[51] However, as the tensile strain on substrate increases further, the force on a FA gets too large and a FA should eventually become less stable or partially damaged, termed as phase III.

Cellular orientation generally coincides with that of SFs. By assuming that FAs would drag the coupled SF to slide or rotate to the direction where they are most stable,[49] we predicted the cellular reorientation when the substrate is subjected to a static biaxial stretch. Consider a SF oriented at an angle θ on a substrate (Figure 5c). The substrate is subjected to a biaxial stretch, with ε_{xx} being the normal strain along the x direction and ε_{yy} the normal strain along the y direction. The tensional modulus of the SF is EA. In the local coordinates, $x'oy'$, where the x' should be parallel to red lines in Figure 5c and coincide with the axial direction of the SF, the strain along the x' direction is

$$\varepsilon_{x'x'} = \varepsilon_{xx}(\cos^2\theta - r\sin^2\theta) \tag{3}$$

where $r = -\varepsilon_{yy}/\varepsilon_{xx}$. For uniaxial tension, r will be exactly the Poisson's ratio. Here we only consider $r > 0$. Due to relatively high flexibility of a SF, ∼1 pN/nm,[49] we regard that $\varepsilon_{x'x'}$ in the substrate is completely transmitted to the SF via FAs. The strain within the SF is initially at its homeostasis state, ε_0.

According to eq 1, the maximum of $\varepsilon_{x'x'}$, which is equal to ε_{xx}, takes place at 0° or 180°. The maximal relaxation strain of a SF due to lengthening is denoted as ε_r. If $\varepsilon_{xx} \le \varepsilon_r$, the extra force built within the SF will be completely relaxed through lengthening, i.e., at phase I. There will be a trivial effect on the stability of FAs. Thus, cellular orientation hardly changes under this condition. F_s denotes the force upon which FAs are most stable. Let $\varepsilon_s = F_s/EA$. If $\varepsilon_r < \varepsilon_{xx} \le \varepsilon_c$, where $\varepsilon_c = \varepsilon_r + \varepsilon_s - \varepsilon_0$, the response of FAs with certain cellular orientation would be at phase II. Under this condition, the FAs at 0° or 180° are most stable, where the force on them is the largest.

If $\varepsilon_c < \varepsilon$, the response of FAs with certain cellular orientation would be at phase III. For example, the FAs at 0° or 180° will become less stable. Under this condition, it can be shown that the most stable FAs exists at

$$\bar{\theta} = \frac{1}{2}\cos^{-1}\left(\frac{2}{1+r}\frac{\varepsilon_c}{\varepsilon_{xx}} - \frac{1-r}{1+r}\right) \quad \text{or}$$
$$= \pi - \frac{1}{2}\cos^{-1}\left(\frac{2}{1+r}\frac{\varepsilon_c}{\varepsilon_{xx}} - \frac{1-r}{1+r}\right) \tag{4}$$

where the force within the SF is equal to F_s. One branch of $\bar{\theta}$ is plotted in Figure 5d–f, which shows its dependence on ε, r, and ε_c. As the static substrate stretch gets larger, the cell reorients further away from the x axis, which is in consistency with the experiments. Our experiemental data indicate that ε_r is less than 10% and $\varepsilon_c \sim 13\%$. The neglect of the effect of cell–cell adhesion or shear strain in the substrate may have led to some deviation of our prediction from the experiments.

Gradients in the mechanical environment (e.g., stiffness and stress/strain) widely exist in native tissues, which play a critical role in regulating cellular behaviors and provide certain structures with specific properties to perform particular tissue functions. Thus, it is neccassary to construct a graded

DOI: 10.1021/acsami.5b04450
ACS Appl. Mater. Interfaces 2015, 7, 15088−15097

mechanical environment in vitro for applications in cell mechanics, tissue remodeling, and tissue engineering. Existing studies produced a large body of knowledge and provided valuable insights into fabricating environment in vitro with stiffness gradients through various approaches including microfluidic and photolithography method. However, to our knowledge, no existing method has been developed to engineer a stress/strain gradient environment with such structures and further study their influence on cell functions. Our strategy may be employed to address this issue. For example, we can obtain a wide range of stress/strain gradient properties by using trapezoidal shaped hydrogels with a long-range length. Additionaly, stress/strain gradients can be easily regulated by programming the hydrogel's shapes. We also use this platform for the first time to precisely engineer cellular alignment gradients in vitro, which is well-known to exert significant effects on tissue regeneration (e.g., neuron) and modulate mechanical properties of tissues including skeleton, cardiac muscle, and tendon.

4. CONCLUSIONS

In summary, we here developed a simple and feasible method to engineer patterned cellular alignment in vitro. Programmable stress/strain gradients on GelMA hydrogels are realized by stretching hydrogels with linear elastic property. When seeding cells on such hydrogels subjected to static stretches, we find that cells on hydrogels align almost perpendicularly to the stretch direction in regions of large strains and gradually align toward the stretch direction in regions of relatively small strains, whereas cells orient randomly in the control group. The effect of substrate strains on cellular alignment is explained with the theory by assuming that FAs would drive the cell to reorient to the directions where they are most stable. Such results indicated that the strain distribution of the substrate significantly and precisely influences the cytoskeleton organization and alignment of cells, which may support a better understanding toward the role of SFs and FAs in response to the deformation of external substrates. In addition, the model system first enabled us to find that, for static stretching, cells only predominantly orient in the constraint direction in a specific uniform strain range (~10% to 13%), in which cellular orientation is a stable phase and supports that cells align to the direction of maximal effective stiffness.[52] For hydrogels with strain gradients in the range of ~13% to 20%, cell alignment is totally in disagreement with the findings from corresponding 2D model systems[53,54] and regulated by the strain of the substrate. We provide here a novel framework for addressing and understanding the response of cellular alignment toward strain gradients of the substrate. The current work not only provides important insights into the cellular response to the local mechanical microenvironment for understainding cellular mechanosensitivity but can also be utilized to engineer patterned cellular alignment that can be critical in tissue remodeling and regeneration.

■ ASSOCIATED CONTENT

Supporting Information

Figures showing gradient hydrogels swelling characterization, cellular alignment generated on gradient hydrogels, and analysis of cellular alignment generated on gradient hydrogels and text describing the theoretical design of the elementary mechanical gradients. These materials are available free of charge via the Internet at The Supporting Information is available free of charge on the ACS Publications website at DOI: 10.1021/acsami.5b04450.

■ AUTHOR INFORMATION

Corresponding Author

*E-mail: fengxu@mail.xjtu.edu.cn.

Author Contributions

⊥L.W. and Y.L. contributed equally to this work.

Notes

The authors declare no competing financial interest.

■ ACKNOWLEDGMENTS

This work was financially supported by the National Natural Science Foundation of China (Grant 11372243 and 11372279), the Natural Science Basic Research Plan in Shaanxi Province of China (Grant 2015JQ1009), the International Science & Technology Cooperation Program of China (Grant 2013DFG02930), the Fundamental Research Funds for the Central Universities (Grant 2013QNA4045), and the Key Program for International S&T Cooperation Projects of Shaanxi (Grant 2013KW33-01 and 2014KW12-01). F.X. was also partially supported by the China Young 1000-Talent Program and Program for New Century Excellent Talents in University (Grant NCET-12-0437). This work was performed at the Bioinspired Engineering and Biomechanics Center (BEBC) at Xi'an Jiaotong University.

■ REFERENCES

(1) Gokhin, D. S.; Fowler, V. M. A Two-Segment Model for Thin Filament Architecture in Skeletal Muscle. *Nat. Rev. Mol.Cell. Biol.* **2013**, *14*, 113−119.

(2) Rehfeldt, F.; Engler, A. J.; Eckhardt, A.; Ahmed, F.; Discher, D. E. Cell Responses to the Mechanochemical Microenvironment-Implications for Regenerative Medicine and Drug Delivery. *Adv. Drug Delivery Rev.* **2007**, *59*, 1329−1339.

(3) Etemad-Moghadam, B.; Guo, S.; Kemphues, K. J. Asymmetrically Distributed PAR-3 Protein Contributes to Cell Polarity and Spindle Alignment in Early C. Elegans Embryos. *Cell* **1995**, *83*, 743−752.

(4) Chew, S. Y.; Mi, R.; Hoke, A.; Leong, K. W. The Effect of the Alignment of Electrospun Fibrous Scaffolds on Schwann Cell Maturation. *Biomaterials* **2008**, *29*, 653−661.

(5) Li, Y.; Huang, G.; Zhang, X.; Wang, L.; Du, Y.; Lu, T. J.; Xu, F. Engineering Cell Alignment in Vitro. *Biotechnol. Adv.* **2014**, *32*, 347−365.

(6) Hoehme, S.; Brulport, M.; Bauer, A.; Bedawy, E.; Schormann, W.; Hermes, M.; Puppe, V.; Gebhardt, R.; Zellmer, S.; Schwarz, M.; Bockamp, E.; Timmel, T.; Hengstler, J. G.; Drasdo, D. Prediction and Validation of Cell Alignment along Microvessels as Order Principle to Restore Tissue Architecture in Liver Regeneration. *Proc. Natl. Acad. Sci. U. S. A.* **2010**, *107*, 10371−10376.

(7) Lutolf, M. P.; Gilbert, P. M.; Blau, H. M. Designing Materials to Direct Stem-Cell Fate. *Nature* **2009**, *462*, 433−441.

(8) Mauriello, E. M. F.; Astling, D. P.; Sliusarenko, O.; Zusman, D. R. Localization of a Bacterial Cytoplasmic Receptor is Dynamic and Changes with Cell-Cell Contacts. *Proc. Natl. Acad. Sci. U. S. A.* **2009**, *106*, 4852−4857.

(9) Blakely, B. L.; Dumelin, C. E.; Trappmann, B.; McGregor, L. M.; Choi, C. K.; Anthony, P. C.; Duesterberg, V. K.; Baker, B. M.; Block, S. M.; Liu, D. R.; Chen, C. S. A DNA-Based Molecular Probe for Optically Reporting Cellular Traction Forces. *Nat. Methods* **2014**, *11*, 1229−1232.

(10) Roux, K. J.; Crisp, M. L.; Liu, Q.; Kim, D.; Kozlov, S.; Stewart, C. L.; Burke, B. Nesprin 4 is an Outer Nuclear Membrane Protein That Can Induce Kinesin-Mediated Cell Polarization. *Proc. Natl. Acad. Sci. U. S. A.* **2009**, *106*, 2194−2199.

DOI: 10.1021/acsami.5b04450
ACS Appl. Mater. Interfaces 2015, 7, 15088−15097

(11) Hoffman, B. D.; Grashoff, C.; Schwartz, M. A. Dynamic Molecular Processes Mediate Cellular Mechanotransduction. *Nature* **2011**, *475*, 316−323.
(12) Jeong, S. I.; Kwon, J. H.; Lim, J. I.; Cho, S.-W.; Jung, Y.; Sung, W. J.; Kim, S. H.; Kim, Y. H.; Lee, Y. M.; Kim, B.-S.; Choi, C. Y.; Kim, S.-J. Mechano-Active Tissue Engineering of Vascular Smooth Muscle Using Pulsatile Perfusion Bioreactors and Elastic PLCL Scaffolds. *Biomaterials* **2005**, *26*, 1405−1411.
(13) Friedl, P.; Sahai, E.; Weiss, S.; Yamada, K. M. New Dimensions in Cell Migration. *Nat. Rev. Mol.Cell. Biol.* **2012**, *13*, 743−747.
(14) Koonin, E. V.; Mulkidjanian, A. Y. Evolution of Cell Division: From Shear Mechanics to Complex Molecular Machineries. *Cell* **2013**, *152*, 942−944.
(15) Oda, H.; Konno, T.; Ishihara, K. The Use of the Mechanical Microenvironment of Phospholipid Polymer Hydrogels to Control Cell Behavior. *Biomaterials* **2013**, *34*, 5891−5896.
(16) Hopp, I.; Michelmore, A.; Smith, L. E.; Robinson, D. E.; Bachhuka, A.; Mierczynska, A.; Vasilev, K. The Influence of Substrate Stiffness Gradients on Primary Human Dermal Fibroblasts. *Biomaterials* **2013**, *34*, 5070−5077.
(17) Tseng, P.; Di Carlo, D. Substrates with Patterned Extracellular Matrix and Subcellular Stiffness Gradients Reveal Local Biomechanical Responses. *Adv. Mater.* **2014**, *26*, 1242−1247.
(18) Polacheck, W. J.; Charest, J. L.; Kamm, R. D. Interstitial Flow Influences Direction of Tumor Cell Migration through Competing Mechanisms. *Proc. Natl. Acad. Sci. U. S. A.* **2011**, *108*, 15−20.
(19) Wang, L.; Li, Y.; Huang, G.; Zhang, X.; Belinda, M.; Xu, F. Hydrogel Based Methods for Engineering Cellular Microenvironment with Spatiotemporal Gradients. *Crit. Rev. Biotechnol.* **2014**, DOI: 10.3109/07388551.2014.993588.
(20) Chan-Park, M. B.; Shen, J. Y.; Cao, Y.; Xiong, Y.; Liu, Y.; Rayatpisheh, S.; Kang, G. C.; Greisler, H. P. Biomimetic Control of Vascular Smooth Muscle Cell Morphology and Phenotype for Functional Tissue-Engineered Small-Diameter Blood Vessels. *J. Biomed. Mater. Res., Part A* **2009**, *88*, 1104−1121.
(21) Zhao, Y.; Zeng, H.; Nam, J.; Agarwal, S. Fabrication of Skeletal Muscle Constructs by Topographic Activation of Cell Alignment. *Biotechnol. Bioeng.* **2009**, *102*, 624−631.
(22) Morioka, M.; Parameswaran, H.; Naruse, K.; Kondo, M.; Sokabe, M.; Hasegawa, Y.; Suki, B.; Ito, S. Microtubule Dynamics Regulate Cyclic Stretch-Induced Cell Alignment in Human Airway Smooth Muscle Cells. *PLoS One* **2011**, *6*, No. e26384.
(23) Helm, P.; Beg, M. F.; Miller, M. I.; Winslow, R. L. Measuring and Mapping Cardiac Fiber and Laminar Architecture Using Diffusion Tensor MR Imaging. *Ann. N. Y. Acad. Sci.* **2005**, *1047*, 296−307.
(24) Sant, S.; Hancock, M. J.; Donnelly, J. P.; Iyer, D.; Khademhosseini, A. Biomimetic Gradient Hydrogels for Tissue Engineering. *Can. J. Chem. Eng.* **2010**, *88*, 899−911.
(25) Keenan, T. M.; Folch, A. Biomolecular Gradients in Cell Culture Systems. *Lab Chip* **2008**, *8*, 34−57.
(26) Alvarado-Velez, M.; Pai, S. B.; Bellamkonda, R. V. Hydrogels as Carriers for Stem Cell Transplantation. *IEEE Trans. Biomed. Eng.* **2014**, *61* (5), 1474−1481.
(27) Li, Y.; Huang, G.; Zhang, X.; Li, B.; Chen, Y.; Lu, T.; Lu, T. J.; Xu, F. Magnetic Hydrogels and Their Potential Biomedical Applications. *Adv. Funct. Mater.* **2013**, *23*, 660−672.
(28) Huang, G.; Wang, L.; Wang, S.; Han, Y.; Wu, J.; Zhang, Q.; Xu, F.; Lu, T. J. Engineering Three-Dimensional Cell Mechanical Microenvironment with Hydrogels. *Biofabrication* **2012**, *4*, No. 042001.
(29) Berthier, E.; Beebe, D. J. Gradient Generation Platforms: New Directions for an Established Microfluidic Technology. *Lab Chip* **2014**, *14*, 3241−3247.
(30) Du, Y.; Hancock, M. J.; He, J.; Villa-Uribe, J. L.; Wang, B.; Cropek, D. M.; Khademhosseini, A. Convection-Driven Generation of Long-Range Material Gradients. *Biomaterials* **2010**, *31*, 2686−2694.
(31) Du, Y.; Shim, J.; Vidula, M.; Hancock, M. J.; Lo, E.; Chung, B. G.; Borenstein, J. T.; Khabiry, M.; Cropek, D. M.; Khademhosseini, A. Rapid Generation of Spatially and Temporally Controllable Long-Range Concentration Gradients in a Microfluidic Device. *Lab Chip* **2009**, *9*, 761−767.
(32) Chao, P. K.; Chan, H. L.; Wang, C. L.; Wu, L. S. Patterns of Left Ventricular Contraction in Strain Vector Space Related to Bundle Branch Block with Heart Failure by Speckle-Tracking Echocardiography. *Ultrasound Med. Biol.* **2011**, *37*, 595−604.
(33) Kunzelman, K. S.; Cochran, R. P. Stress/Strain Characteristics of Porcine Mitral Valve Tissue: Parallel Versus Perpendicular Collagen Orientation. *J. Cardiac Surg.* **1992**, *7*, 71−78.
(34) Gupta, V.; Tseng, H.; Lawrence, B. D.; Grande-Allen, K. J. Effect of Cyclic Mechanical Strain on Glycosaminoglycan and Proteoglycan Synthesis by Heart Valve Cells. *Acta Biomater.* **2009**, *5*, 531−540.
(35) Sengupta, P. P.; Narula, J. Cardiac Strain as a Universal Biomarker: Interpreting the Sounds of Uneasy Heart Muscle Cells. *JACC: Cardiovasc. Imaging* **2014**, *7*, 534−536.
(36) Hu, Y. H.; Suo, Z. G. Viscoelasticity and Poroelasticity in Elastomeric Gels. *Acta Mech. Solida Sin.* **2012**, *25*, 441−458.
(37) Jeon, O.; Alt, D. S.; Linderman, S. W.; Alsberg, E. Biochemical and Physical Signal Gradients in Hydrogels to Control Stem Cell Behavior. *Adv. Mater.* **2013**, *25*, 6366−6372.
(38) Hsieh, H. Y.; Camci-Unal, G.; Huang, T. W.; Liao, R.; Chen, T. J.; Paul, A.; Tseng, F. G.; Khademhosseini, A. Gradient Static-Strain Stimulation in a Microfluidic Chip for 3D Cellular Alignment. *Lab Chip* **2014**, *14*, 482−493.
(39) Olsen, M. H.; Hjorto, G. M.; Hansen, M.; Met, O.; Svane, I. M.; Larsen, N. B. In-Chip Fabrication of Free-Form 3D Constructs for Directed Cell Migration Analysis. *Lab Chip* **2013**, *13*, 4800−4809.
(40) Fan, Y.; Xu, F.; Huang, G.; Lu, T. J.; Xing, W. Single neuron capture and axonal development in three-dimensional microscale hydrogels. *Lab Chip* **2012**, *12*, 4724−4731.
(41) Gurkan, U. A.; Fan, Y.; Xu, F.; Erkmen, B.; Urkac, E. S.; Parlakgul, G.; Bernstein, J.; Xing, W.; Boyden, E. S.; Demirci, U. Simple Precision Creation of Digitally Specified, Spatially Heterogeneous, Engineered Tissue Architectures. *Adv. Mater.* **2013**, *25*, 1192−1198.
(42) Zhao, R. G.; Boudou, T.; Wang, W. G.; Chen, C. S.; Reich, D. H. Decoupling Cell and Matrix Mechanics in Engineered Microtissues Using Magnetically Actuated Microcantilevers. *Adv. Mater.* **2013**, *25*, 1699−1705.
(43) Cheung, W.; Hamarneh, G. N-SIFT: N-dimensional Scale Invariant Feature Transform. *IEEE Trans. Image Process.* **2009**, *18*, 2012−2021.
(44) Xu, F.; Beyazoglu, T.; Hefner, E.; Gurkan, U. A.; Demirci, U. Automated and Adaptable Quantification of Cellular Alignment from Microscopic Images for Tissue Engineering Applications. *Tissue Eng., Part C* **2011**, *17*, 641−649.
(45) McKee, C. T.; Last, J. A.; Russell, P.; Murphy, C. J. Indentation Versus Tensile Measurements of Young's Modulus for Soft Biological Tissues. *Tissue Eng., Part. B* **2011**, *17*, 155−164.
(46) Loesberg, W. A.; Walboomers, X. F.; van Loon, J. J.; Jansen, J. A. The Effect of Combined Cyclic Mechanical Stretching and Micro-grooved Surface Topography on the Behavior of Fibroblasts. *J. Biomed. Mater. Res., Part A* **2005**, *75*, 723−732.
(47) Wang, J. H.; Yang, G.; Li, Z.; Shen, W. Fibroblast Responses to Cyclic Mechanical Stretching Depend on Cell Orientation to the Stretching Direction. *J. Biomech.* **2004**, *37*, 573−576.
(48) Tan, W.; Scott, D.; Belchenko, D.; Qi, H. J.; Xiao, L. Development and Evaluation of Microdevices for Studying Anisotropic Biaxial Cyclic Stretch on Cells. *Biomed. Microdevices* **2008**, *10*, 869−882.
(49) Chen, B.; Kemkemer, R.; Deibler, M.; Spatz, J.; Gao, H. J. Cyclic Stretch Induces Cell Reorientation on Substrates by Destabilizing Catch Bonds in Focal Adhesions. *PLoS One* **2012**, *7*, No. e48346.
(50) Hill, A. V. The Heat of Shortening and the Dynamic Constants of Muscle. *Proc. R. Soc. London, Ser. B* **1938**, *126*, 136−195.
(51) Balaban, N. Q.; Schwarz, U. S.; Riveline, D.; Goichberg, P.; Tzur, G.; Sabanay, I.; Mahalu, D.; Safran, S.; Bershadsky, A.; Addadi, L.; Geiger, B. Force and Focal Adhesion Assembly: A Close

DOI: 10.1021/acsami.5b04450
ACS Appl. Mater. Interfaces 2015, 7, 15088−15097

Relationship Studied using Elastic Micropatterned Substrates. *Nat. Cell Biol.* **2001**, *3*, 466−472.
(52) Foolen, J.; Deshpande, V. S.; Kanters, F. M. W.; Baaijens, F. P. T. The Influence of Matrix Integrity on Stress-Fiber Remodeling in 3D. *Biomaterials* **2012**, *33*, 7508−7518.
(53) Rubbens, M. P.; Driessen-Mol, A.; Boerboom, R. A.; Koppert, M. M. J.; van Assen, H. C.; Romeny, B. M. T.; Baaijens, F. P. T.; Bouten, C. V. C. Quantification of the Temporal Evolution of Collagen Orientation in Mechanically Conditioned Engineered Cardiovascular Tissues. *Ann. Biomed. Eng.* **2009**, *37*, 1263−1272.
(54) Boerboom, R. A.; Rubbens, M. P.; Driessen, N. J. B.; Bouten, C. V. C.; Baaijens, F. P. T. Effect of Strain Magnitude on the Tissue Properties of Engineered Cardiovascular Constructs. *Ann. Biomed. Eng.* **2008**, *36*, 244−253.

DOI: 10.1021/acsami.5b04450
ACS Appl. Mater. Interfaces 2015, 7, 15088−15097